



**HAL**  
open science

# Nonmonotonic Response of Primary Production and Export to Changes in Mixed-Layer Depth in the Southern Ocean

Joan Llort, Marina Lévy, Jean-Baptiste Sallée, Alessandro Tagliabue

► **To cite this version:**

Joan Llort, Marina Lévy, Jean-Baptiste Sallée, Alessandro Tagliabue. Nonmonotonic Response of Primary Production and Export to Changes in Mixed-Layer Depth in the Southern Ocean. *Geophysical Research Letters*, 2019, 46 (6), pp.3368-3377. 10.1029/2018GL081788 . hal-02117445

**HAL Id: hal-02117445**

**<https://hal.science/hal-02117445v1>**

Submitted on 27 Nov 2020

**HAL** is a multi-disciplinary open access archive for the deposit and dissemination of scientific research documents, whether they are published or not. The documents may come from teaching and research institutions in France or abroad, or from public or private research centers.

L'archive ouverte pluridisciplinaire **HAL**, est destinée au dépôt et à la diffusion de documents scientifiques de niveau recherche, publiés ou non, émanant des établissements d'enseignement et de recherche français ou étrangers, des laboratoires publics ou privés.

1 **Non-monotonic response of primary production and export to changes in**  
2 **mixed-layer depth in the Southern Ocean**

3 J. Llorc<sup>1,2</sup>, M. Lévy<sup>3</sup>, J.B.Sallée<sup>3</sup> and A.Tagliabue<sup>4</sup>

4

5 <sup>1</sup> Institute of Marine and Antarctic Studies, University of Tasmania, Hobart, Australia

6 <sup>2</sup> Australian Research Council Centre of Excellence for Climate System Science, Hobart,  
7 Tasmania, Australia

8 <sup>3</sup> Sorbonne Université, LOCEAN-IPSL, CNRS/IRD/MNHN, Paris, France

9 <sup>4</sup> School of Environmental Sciences, University of Liverpool, UK

10 Corresponding author: Joan Llorc (jllorc@utas.edu.au)

11 **Key Points:**

- 12 • Moderate shoaling of winter mixed layer causes increase in primary production but  
13 shoaling below a threshold depth can lead to a collapse.
- 14 • Reversal in this response is due to balancing effects of iron and light limitation and  
15 associated with a change in community structure and export efficiency.
- 16 • Interestingly, shoaling summer mixed layer always reduces PP and export because of a  
17 reduction of the productive volume.

18

19 **Abstract**

20 Ongoing and future changes in wind and temperature are predicted to alter upper ocean vertical  
21 mixing across the Southern Ocean. How these changes will affect primary production (PP)  
22 remains unclear as mixing influences the two controlling factors: light and iron. We used a large  
23 ensemble of 1D-biogeochemical model simulations to explore the impacts of changes in mixed-  
24 layer depths (MLD) on PP in the Southern Ocean. In summer, shoaling MLD always reduced  
25 depth-integrated PP, despite increasing production rates. In winter, shoaling mixed-layers had a  
26 two-staged impact: for moderate shoaling PP increased as light conditions improved, but more  
27 pronounced shoaling decreased iron supply, which reduced PP. The fraction of PP exported  
28 below 100m also presented a non-monotonic behavior. This suggests a potential future shift from  
29 a situation where reduced winter mixing increases PP and export, to a situation where PP and  
30 export may collapse if the ML shoals above a threshold depth.

31

32 **Plain Language Summary**

33 In the Southern Ocean, atmospheric warming associated to climate change is altering the depth at  
34 which surface waters are stirred, the so-called *mixed-layer depth*. A change in the *mixed-layer*  
35 *depth* impacts the phytoplankton cells that inhabit it by altering their two main limiting factors:  
36 iron and light. However, the sign and magnitude of this impact are still not clear. In this work we  
37 used mathematical simulations to explain how changes in the seasonal *mixed-layer depth* modify  
38 the supply of iron and the amount of light, and how these changes impact phytoplankton activity.  
39 Our results show that *mixed-layer depth* changes in summer and in winter have different impacts.  
40 Reducing summer *mixed-layer depth* did not change the iron supply but it reduced the volume of  
41 water where phytoplankton thrived. In winter, shallower *mixed-layer depth* altered iron and light  
42 but in opposed ways. At first, phytoplankton increased its activity as more light became  
43 available. However, a continued shallowing of the *mixed-layer depth* eventually reduced the iron  
44 supply and the phytoplankton activity. Our study proposes a new interpretation on how ongoing  
45 changes in the Southern Ocean impact phytoplankton activity and alerts of the presence of  
46 threshold depths for the winter mixed-layer above which phytoplankton may struggle to survive.

47

## 48 **1 Introduction**

49 Southern Ocean (SO) atmospheric and oceanic conditions are currently changing in response to  
50 increasing atmospheric concentrations of greenhouse gases and changes in the concentration of  
51 stratospheric ozone (Swart et al, 2018). Model projections from the fifth phase of the Coupled  
52 Model Intercomparison Project (CMIP5, Taylor et al., 2012) highlight a changing wind pattern  
53 associated with a more persistent phase of the Southern Annular Mode (SAM), together with  
54 warmer sea-surface temperature north of the sea-ice zone (Bracegirdle et al., 2013; Cai et al,  
55 2003; Swart et al, 2015; Zheng et al, 2013). Such changes in the physical environment are  
56 expected to affect the capacity of phytoplankton to fix atmospheric carbon, their community  
57 composition and the overall efficiency of the biological carbon pump (Lenton and Matear, 2007;  
58 Lovenduski and Gruber, 2005). In particular, it is critical to understand how physical changes  
59 will alter iron and light availability, as these two elements play fundamental roles in structuring  
60 the response of phytoplankton communities (Boyd et al, 2002).

61 In a recent review, Deppeler and Davidson (2017) identified a large number of factors able to  
62 alter primary production in the Southern Ocean. Amongst these factors, changes in the seasonal  
63 mixed-layer depth (MLD) were particularly important north of the sea-ice zone. However,  
64 neither the sign nor the magnitude of change are yet clear due to the complex links between the  
65 seasonal cycle of the MLD and primary production in the Southern Ocean. Two reasons  
66 contribute to this complexity. First, the sign of the change in MLD is expected to vary regionally  
67 and seasonally, depending on changes in surface warming, wind and freshwater fluxes (Panassa  
68 et al, 2018, Sallée et al, 2013). Second, vertical mixing plays a complex role for phytoplankton,  
69 since shallow MLDs may maintain cells in the well-lit part of the water column, but, at the same  
70 time, the vertical extent of the upper mixing layer controls the vertical supply of iron from  
71 deeper reserves. Thus, while a decrease in MLD enhances productivity in light limited conditions  
72 through the first mechanism, it reduces productivity through the second mechanism in regions  
73 where iron is supplied by vertical mixing in winter (Doney, 2006; Sarmiento et al, 2004). In this  
74 second case, the winter supply of iron is more efficient when the mixed-layer deepens within the  
75 subsurface iron reservoir (hereafter, we refer to the upper limit of the iron reservoir as the  
76 ferricline, see methods for details). The two mechanisms described by this paradigm are  
77 concomitant in the Southern Ocean, where both light limitation and iron limitation co-exist in

78 time and space (Boyd et al 2010). Moreover, given that such interplay varies throughout the  
79 seasonal cycle, changes in the seasonal extremes of the MLD in winter and summer ( $MLD_{winter}$   
80 and  $MLD_{summer}$ , respectively) are expected to have different impacts on annual values of primary  
81 production (Deppeler and Davidson, 2017, Hauck et al, 2015).

82 End-of-century projections from CMIP5 show a coherent latitudinal pattern of change in primary  
83 production over the Southern Ocean (Bopp et al, 2013; Laufkötter et al, 2015). In the 30°-40°S  
84 latitudinal band CMIP5 models agree on a nutrient-driven decrease in primary production as a  
85 consequence of the broadening of oligotrophic gyres to southern waters (Hauck et al, 2015). In  
86 the 40°-50°S latitudinal band, models project an increase in primary production, followed by a  
87 decrease in the 50°-65°S band (Bopp et al 2013). Leung et al. (2015) found a consistent response  
88 between models on the primary production increase at 40°-50°S. Their analysis associated the  
89 change in primary production to a reduction of  $MLD_{summer}$  combined with an increase in surface  
90 iron. Alternatively, the primary production decrease in the 50°-65°S band was not consistent  
91 between models and has been linked to deeper  $MLD_{summer}$  combined with a reduction of the  
92 incident photosynthetically available radiation. However, the mechanisms behind these changes  
93 remain unclear as projected patterns have only been explained through correlation relationships  
94 (Leung et al, 2015), or masked by the strong primary production increase associated to Antarctic  
95 sea-ice decline (Laufkötter et al, 2015). The overlap between different drivers in climate models  
96 does not allow evaluating the influence of changes in MLD alone over primary production.  
97 Furthermore, the uncertainties in these models are likely to induce incorrect interpretations based  
98 on theoretical paradigms (Lovenduski and Gruber, 2005). The largest uncertainty is caused by  
99 the inability of CMIP5 models to correctly reproduce dissolved iron and MLD observations in  
100 the Southern Ocean (Sallée et al, 2015; Tagliabue et al, 2016), particularly in winter. These  
101 uncertainties cascade into the iron vertical supply and cause a model-dependent biogeochemical  
102 response in the Southern Ocean (Schourup-Kristensen, 2014).

103 Moreover, the lack of mechanistic understanding and the uncertainties associated to primary  
104 production drivers in the Southern Ocean also impact the estimates of how much carbon is  
105 eventually transferred into the deep ocean. The export of carbon depends on a number of  
106 processes such as the plankton community structure, remineralization rates, temperature or MLD  
107 variability (Boyd and Trull, 2007; Henson et al, 2015). The disparities on how biogeochemical

108 models resolve these mechanisms add up to iron supply uncertainties and cause a lack of  
109 agreement between climate-models in the Southern Ocean (Laufkötter et al, 2016). This lack of  
110 consensus is particularly severe in the mid-latitudes, 44°-58°S (Hauck et al, 2015).

111 A number of observation-based studies provide evidences that in the Southern Ocean the two  
112 aspects of the primary production-MLD paradigm (Fig 1 in Doney, 2006) might be occurring  
113 simultaneously. Ardyna et al. (2017) combined data from satellite ocean-color with Argo floats  
114 to show that regional variability in Southern Ocean phytoplankton biomass results from a mixed  
115 balance of drivers in addition to light, including the proximity to island or submerged seamounts,  
116 sea-ice, or  $MLD_{winter}$ . Interestingly, they show that, away from specific iron sources,  
117 phytoplankton biomass increases as a function of  $MLD_{winter}$ , for  $MLD_{winter}$  ranging from 0 to  
118 ~150m, but decreases for  $MLD_{winter} > 150m$ . They interpret the presence of such a regime shift  
119 as a transition from an iron-limited environment (shallow  $MLD_{winter}$ ) to a light-limited  
120 environment (deep  $MLD_{winter}$ ). Similarly, Hoppe et al. (2017) reported strong blooming  
121 conditions in regions of deep mixing, suggesting a secondary role of light limitation on  
122 controlling summer production. This result agrees with Venables and Moore (2010) who found  
123 no influence of light limitation over the annual integrated chlorophyll-a in Southern Ocean  
124 waters.

125 In this paper, we investigate how ongoing and future changes in winter and summer MLD may  
126 influence primary production and the export of organic carbon with a modeling configuration  
127 specifically designed to address this question in the context of the Southern Ocean. Our approach  
128 avoids the complexity related to climate models and, at the same time, captures the double-role  
129 of the MLD on primary production. To do so, we implemented a state-of-the-art biogeochemical  
130 model into a fully controlled one-dimensional (1D) physical configuration. We varied  $MLD_{winter}$ ,  
131  $MLD_{summer}$  and ferricline depth ( $Z_{Fe}$ ) along typical present and projected ranges for the Southern  
132 Ocean. Despite the idealized approach, the statistical analysis of a large ensemble (752) of  
133 simulated annual cycles showed a complex relationship between MLD, primary production and  
134 export. Our results challenge current interpretations of CMIP5 projections in the Southern Ocean  
135 and propose the presence of a threshold depth for  $MLD_{winter}$  below which production would  
136 collapse.

## 137 2. Methods

138 Our model configuration represents an ocean water column resolved as a vertical grid of 75  
139 equally spaced cells. Only vertical exchanges are considered (i.e., it is a 1D configuration). The  
140 same configuration was used in Llorc et al. (2015) to study the bloom phenology in the SO and is  
141 fully described therein; here we recall the fundamental model characteristics. We use the  
142 biogeochemical model PISCES (Aumont and Bopp, 2006) that we force with three physical  
143 variables: surface solar short-wave radiation, temperature and turbulent vertical mixing ( $\kappa_z$ ).  
144 These three variables are prescribed and follow a complete seasonal cycle starting on the 15th of  
145 February. The vertical profile of  $\kappa_z$  is set as a step-like function, with a value of  $1 \text{ m}^2 \text{ s}^{-1}$  within  
146 an upper mixed-layer and a small open ocean mixing of  $10^{-5} \text{ m}^2 \text{ s}^{-1}$  (Cisewski et al, 2005) below  
147 the mixed-layer. The strong mixing in the upper layer ensures a homogenous vertical distribution  
148 of phytoplankton and nutrients (Lévy, 2015). The depth of the surface mixed-layer (and thus the  
149 penetration depth of strong vertical mixing) varies along an idealized seasonal cycle consisting  
150 of three phases (Fig 1a,b): a first phase of linear deepening until the maximum depth ( $\text{MLD}_{\text{winter}}$ ,  
151 from 15th February to 15th September), a second phase of linear shoaling (from 15th September  
152 to 15th December) and a period of constant depth in summer ( $\text{MLD}_{\text{summer}}$ , 15th December to 14th  
153 February of the next year).

154 PISCES contains 24 biogeochemical tracers, among which five nutrients (nitrate, phosphate,  
155 ammonium, iron, and silicate), two phytoplankton size classes (small and large) and two  
156 zooplankton size classes (micro-zooplankton and meso-zooplankton). Large phytoplankton  
157 differs from small phytoplankton by higher iron requirements and a greater iron half-saturation  
158 constant.

159 Initial vertical profiles for macronutrient (i.e. nitrate, phosphate, and silicate) were constructed  
160 based on the winter mean profiles of a typical HNLC region (Jeandel et al., 1998). We carried a  
161 series of sensitivity experiments to ensure that only iron limits phytoplankton growth. The  
162 summer initial condition for dissolved iron profile was constructed by assuming low  
163 concentrations ( $0.03 \text{ nmol Fe l}^{-1}$ ) above a prescribed depth and larger concentrations ( $0.5 \text{ nmol}$   
164  $\text{Fe l}^{-1}$ ) below. The depth where iron concentration suddenly increases is referred here as the  
165 ferricline ( $Z_{\text{Fe}}$ ). Iron supply into the upper mixed layer is not prescribed, but emerges from the



166 vertical entrainment and diffusion of iron, which depends on the respective depth of the  $Z_{Fe}$  and  
167 the MLD. While lateral advection might be another important source of dissolved iron in specific  
168 SO regions, particularly in the lee of islands or continental shelves, it is neglected here to  
169 concentrate on vertical entrainment of iron. Vertical entrainment of iron is likely the dominant  
170 source of iron supply in most of the Southern Ocean, which is characterized by deep ferricline  
171 (Tagliabue et al., 2014). In this study, iron supply is computed as the amount of dissolved iron  
172 that enters MLD.

## 173 **Ensemble of runs**

174 The 1D physical setting forced the PISCES model under current and future MLD conditions. We  
175 conducted an ensemble of simulations where we varied three forcing parameters,  $MLD_{winter}$ ,  
176  $MLD_{summer}$  (Pellichero et al, 2017) and  $Z_{Fe}$  (Tagliabue et al, 2014), over the full range of  
177 observed values in the SO. Values for future MLD were obtained from CMIP5 climate model  
178 projections (Sallée et al, 2013; Taylor et al, 2012). Overall, we prescribed 11 distinct values of  
179  $MLD_{winter}$  (between 100m and 600m), combined with 9 distinct values for  $MLD_{summer}$  (between  
180 20m and 100m) and 8  $Z_{Fe}$  values (between 150 and 500m). The combination of all  $MLD_{winter}$ ,  
181  $MLD_{summer}$  and  $Z_{Fe}$  values resulted in 752 different scenarios. This approach allowed us to  
182 identify how changes in MLD affect primary production and export over a wide range of oceanic  
183 conditions typical of the Southern Ocean.

## 184 **4 Results**

### 185 **4.1 Response to changes in winter MLD**

186 Southern Ocean open waters extend from mid to high-latitudes, with seasons being clearly  
187 differentiated and incident Photosynthetically Available Radiation (PAR) being lower in winter  
188 than in summer. However, the average light received by phytoplankton is lower than surface  
189 PAR as cells are vertically mixed across the mixed-layer. The light used for the photosynthesis  
190 can then be calculated using the PAR attenuation profile averaged across the mixed-layer  
191 ( $PAR_{ML}$ ). Thus, deeper (shallower)  $MLD_{winter}$  reduce (increase)  $PAR_{ML}$ , exacerbating (relaxing)  
192 light limitation of phytoplankton growth and primary production (Boyd et al, 2010).  $MLD_{winter}$   
193 also has an impact on growth and primary production limitation by controlling vertical supply of

194 iron. Deeper  $MLD_{winter}$  tend to drive stronger iron supplies and enhance phytoplankton growth  
195 (Tagliabue et al, 2014). We first examine how the combination of these two opposing  
196 mechanisms (light and iron limitation) drive differences in primary production in three model  
197 simulations that only differ by their  $MLD_{winter}$  values (deep, intermediate and shallow scenario),  
198 with identical  $MLD_{summer}$  and  $Z_{Fe}$  (Fig 1, left panels).

199 From March to July, the seasonal decrease of surface PAR combined with the deepening of the  
200 mixed-layer strongly decreased  $PAR_{ML}$  for all three scenarios (Fig 1a and b).  $PAR_{ML}$  remained  
201 low until October, when the shoaling of the MLD caused a rapid increase (Fig. 1b). The vertical  
202 supply of iron initiated when the mixed-layer depth crossed  $Z_{Fe}$  (Fig 1b). These two factors,  
203  $PAR_{ML}$  and iron supply, acted together to shape the response in primary production (Fig 1c and  
204 d). From March to July, depth-integrated primary production was low and with a decreasing  
205 trend (Fig 1c). For the three scenarios a period of slow increase started around July, and was  
206 followed by a marked bloom in spring.

207 The three simulations exhibited differences in the timing and amplitude of the bloom (Fig. 1c).  
208 In the shallow simulation, winter iron supply was relatively low ( $24 \mu\text{molFe m}^{-2} \text{yr}^{-1}$ ) and the  
209 bloom was the weakest and earliest. Production started increasing on July 1st and peaked in  
210 November, shortly after the mixing layer started shoaling and a month after iron supply ceased  
211 (Fig. 1a, b and c). On the contrary, the bloom in the deep  $MLD_{winter}$  simulation was the strongest  
212 and the slowest to develop of all three scenarios. In this scenario,  $MLD_{winter}$  penetrated deeply  
213 into  $Z_{Fe}$ , which enhanced the vertical flux of iron ( $60 \mu\text{molFe m}^{-2} \text{yr}^{-1}$ ). Nevertheless, integrated  
214 primary production did not increase until the mixed-layer started shoaling in October. The large  
215 amount of accumulated iron during winter and the quick spring increase in  $PAR_{ML}$  supported a  
216 strong, but relatively short bloom, peaking in December.

217 Interestingly, these two extreme simulations led to similar values of annual integrated primary  
218 production ( $74.8 \text{ gC m}^{-2} \text{yr}^{-1}$  for the shallow simulation and  $75.5 \text{ gC m}^{-2} \text{yr}^{-1}$  for the deep  
219 simulation, Fig 1d), yet the relative contributions of small and large phytoplankton were notably  
220 different. The annual primary production supported by the large phytoplankton group  
221 represented 34% of the total production for the iron-poor shallow simulation while for the iron-  
222 rich deep simulation it reached 52% (dashed lines in Fig 1d).

223 When these two end-members simulations are compared to the intermediate  $MLD_{winter}$  scenario a  
224 non-monotonic response of annual primary production to varying  $MLD_{winter}$  emerges. While the  
225 bloom in the intermediate  $MLD_{winter}$  simulation presented intermediate characteristics (iron  
226 supply was  $53 \mu\text{molFe m}^{-2} \text{yr}^{-1}$ , Fig 1c), it showed the highest annual production ( $79.1 \text{ gC m}^{-2} \text{yr}^{-1}$ )  
227 of all three simulations (Fig 1d). The balance between a weak, long-lasting and small-  
228 phytoplankton-dominated winter bloom; and a high, quick and large-phytoplankton-dominated  
229 spring bloom appeared to be optimal in the case of the intermediate experiment.

230 When we analyzed the results from our ensemble of 752 simulations (Fig. 2a), two contrasted  
231 modes emerged in the response of annual primary production (PP) to changes in  $MLD_{winter}$ . The  
232 first mode was associated with a deep iron reservoir ( $Z_{Fe} > 350 \text{ m}$ ), and the second mode with a  
233 shallow iron reservoir ( $Z_{Fe} < 250 \text{ m}$ ). Both modes presented non-monotonic PP- $MLD_{winter}$   
234 relationships: for a given  $Z_{Fe}$ , PP increased as  $MLD_{winter}$  decreased, until  $MLD_{winter}$  reached a  
235 threshold depth ( $Z_{PPmax}$ , indicated by the white contours in Fig. 2a), where the PP- $MLD_{winter}$   
236 relationship reversed and PP started decreasing. The threshold depth marked a local maximum in  
237 PP and depended on the  $Z_{Fe}$  mode. Situations with  $250\text{m} < Z_{Fe} < 350\text{m}$  corresponded to a  
238 transition regime between these two modes, characterized by the presence of two  $Z_{PPmax}$  (dashed  
239 white lines in Fig. 2a).

240 The deep iron reservoir mode presented a relatively shallow  $Z_{PPmax}$ , at around 200 m. In this  
241 mode, iron supplies were systemically low ( $< 10 \mu\text{molFe m}^{-2} \text{yr}^{-1}$ ; black contours in Fig 2a), even  
242 when  $MLD_{winter}$  was deeper than  $Z_{Fe}$  since on those occasions there was only a brief period  
243 where  $MLD$  was deeper than  $Z_{Fe}$ . In contrast, the shallow  $Z_{Fe}$  mode was characterized by  
244 relatively large iron supplies, which were proportional to  $MLD_{winter}$ . In this mode, the threshold  
245 depths were deeper (between 350m and 500m) and depended strongly on  $Z_{Fe}$ .

246 In both modes, the iron supply and the contribution of the large phytoplankton group to total PP  
247 responded monotonically to changes in  $MLD_{winter}$ . This highlights that, as for the example shown  
248 in Fig. 1, the threshold depth of  $MLD_{winter}$  marks a boundary between two different community  
249 responses: for  $MLD_{winter}$  shallower than  $Z_{PPmax}$ , the community is dominated by small-  
250 phytoplankton, and PP of both large and small phytoplankton groups respond monotonically to  
251 changes in iron supply (Fig 2b-c); for  $MLD_{winter}$  deeper than  $Z_{PPmax}$ , the community is dominated

252 by large-phytoplankton, and light becomes the dominant limiting factor, particularly for the  
253 small-phytoplankton group (Fig 2b).

254 The role of zooplankton in these responses was also addressed by diagnosing the percentage of  
255 PP grazed, hereinafter referred as the grazing efficiency. Our simulations show that grazing  
256 efficiency was strongly dependent on the community structure (Fig 2d), as small phytoplankton  
257 is more easily grazed than large phytoplankton. Such dependency suggests a minor role of  
258 zooplankton grazing as it follows the change on community structure, which is in turn caused by  
259 changes in MLD.

260 A further climate-relevant metric associated with marine production is how much of the organic  
261 carbon synthesized in the upper ocean is exported to the deep ocean. Under shallow ferricline  
262 conditions, the amount of production exported below 100m (EP) showed a non-monotonic  
263 response to changing  $MLD_{winter}$  with a threshold depth at 500m (Fig. 3a). EP responded in  
264 parallel to the productivity supported by the larger class of phytoplankton (Fig. 2c) because large  
265 phytoplankton tends to aggregate and sink faster than small phytoplankton (Boyd and Trull,  
266 2007; Laufkötter et al, 2016). In contrast, and unlike PP, under deep ferricline and small  
267 phytoplankton conditions we observed a monotonic response, with a constant increase in export  
268 as  $MLD_{winter}$  decreased (Fig 3a).

#### 269 **4.2 Response to changes in Summer MLD**

270 Phytoplankton growth and primary production rates are the highest during late spring and early  
271 summer as surface waters are replenished with iron and light is abundant (Boyd et al 2010).  
272 Therefore changes in  $MLD_{summer}$ , even if small in magnitude, have the potential to influence  
273 annual productivity (Laufkötter et al, 2015; Leung et al, 2015) and export (Hauck et al, 2015). In  
274 order to understand the mechanisms by which changes in  $MLD_{summer}$  affect primary production,  
275 we first compared three simulations with different values of  $MLD_{summer}$  (20, 50 and 80 meters)  
276 but with,  $Z_{Fe}$  set to 150 meters and  $MLD_{winter}$  at 300m (Fig 1e). Dissolved iron supplies were  
277 very similar among the three simulations but  $PAR_{ML}$  strongly differed, with values nine times  
278 larger in the shallow experiment than in the deep one (Fig 1f). Stronger light limitation in the  
279 deep experiment caused the bloom to be slightly weaker and last longer than in the shallow  
280 experiment (Fig 1g). However, annual primary production was the largest in the deep experiment

281 and this mainly resulted from an increase of the productive volume which caused higher depth-  
282 integrated primary production during summer (Fig 1h), despite having the lowest MLD-averaged  
283 production rates,  $PP_{ML}$  (dashed lines in Fig 1h).

284 The decrease in annual primary production under shallower  $MLD_{summer}$  was consistent amongst  
285 all 752 simulations (Fig. 2e). This response suggested that in our model annual primary  
286 production was not light limited in summer.  $MLD_{summer}$  was always shallower than ferricline  
287 depths and iron supply remained low for all scenarios (black lines in Fig 2 e, f, g). Export  
288 production was less sensitive to changes in  $MLD_{summer}$  than primary production (Fig. 3b), due to  
289 the larger contribution of small phytoplankton cells to productivity under deep  $MLD_{summer}$  (Fig.  
290 2f).

## 291 **5 Discussion and Conclusions**

292 The analysis of our ensemble of model simulations revealed that changes in primary production  
293 driven by changes in mixed-layer depth are more complex than previously thought. The change  
294 in primary production in response to variations in winter mixed-layer was non-monotonous: total  
295 primary production and winter mixed-layer depth were positively correlated for winter mixed-  
296 layer depths above a certain threshold depth (that we refer as  $Z_{PPmax}$ ), but negatively correlated  
297 for winter mixed-layer depths below this threshold (Fig 2a). The  $Z_{PPmax}$  for the mixed-layer  
298 emerged due to the overlap of the two limiting factors, light and iron availability (Fig 1b).  
299 Interestingly,  $Z_{PPmax}$  was related to both the biogeochemical conditions and ecosystem  
300 composition. For instance,  $Z_{PPmax}$  was shallower for iron-poor and small-phytoplankton  
301 dominated conditions than for iron-rich conditions where the two phytoplankton groups  
302 contributed more equally (Fig 2b). Our analysis also shown that, quite unexpectedly, deeper  
303 summer mixed-layers induced larger total primary production, despite lower phytoplankton  
304 growth rates, because of an increase in the productive water volume (Fig 1, right panels and Fig  
305 2a). Lastly, our experiments contribute to an understanding of how changes in MLD can alter the  
306 carbon export. As expected, phytoplankton size composition was crucial to controlling carbon  
307 export (Fig 3a and b). Under conditions of deep winter mixed-layers and iron-rich environments,  
308 decreasing the mixed-layer depth resulted in a reduction of the export by decreasing iron-supply  
309 and the presence of fast-sinking large phytoplankton. However, this trend reversed within

310 environments dominated by small-phytoplankton and export increased with decreasing mixed-  
311 layers. Two combined mechanisms likely controlled this trend. In the first place, a larger portion  
312 of primary production was grazed by zooplankton (Fig 2d), hence more organic matter could be  
313 exported as sinking particles in form of fecal pellets. In the second place, the shallower the  
314 mixed-layer the easier for particles to escape from surface turbulence and sink into the ocean  
315 (Pavelsky and Doney, 2018).

316 These results have consequences on how we understand current and future Southern Ocean  
317 productivity and export. Firstly, because the iron distribution and winter mixed-layer in the  
318 Southern Ocean are zonally asymmetric (Tagliabue et al, 2014), future trends in primary  
319 production and export are also likely to vary in both latitude and longitude. This conclusion  
320 agrees with the observed zonal asymmetries of phytoplankton phenology provinces (Ardyna et  
321 al, 2017) and challenges the prevailing latitudinal pattern of primary production trends projected  
322 by most CMIP5 models (Bopp et al, 2013, Leung et al, 2015). We conclude that the latter is  
323 more likely to be caused by the inability of current climate models to correctly reproduce the  
324 zonal asymmetries in MLD (Sallée et al, 2013) and iron distribution (Schourup-Kristensen, 2015,  
325 Tagliabue et al, 2016). Secondly, the non-monotonic response of primary production to MLD  
326 should be further explored, particularly in observations, in order to evaluate the threshold depth  
327 in winter mixed-layer depth within contrasted bioregions and identify which ecosystems are  
328 closer to collapse. Along this line, Ardyna et al. (2017) estimated an average threshold depth  
329 over the whole Southern Ocean of ~150m (their Fig S2) that can be used as a benchmark for  
330 future studies. From a modeling perspective, evaluating the evolution of trends by decade,  
331 instead of just comparing two extreme decades (i.e. projected against historical) may help  
332 elucidate the non-monotonic responses in CMIP projections. Lastly, summer results suggest that  
333 changes in summer mixed-layer depth do not significantly affect iron supply because the  
334 ferricline depth is always deeper than the deepest plausible range of climatological summer  
335 mixed-layer depth (see Fig 1c in Tagliabue et al, 2014, which shows that the ferricline depth is  
336 deeper than 200m over 75% of the observed summer iron profiles). Summer storms, however,  
337 which have not been accounted for in this study, may be more effective in supplying iron in the  
338 case of deeper summer mixed-layer depths (Carranza and Gille, 2015, Nicholson et al., 2016).

339 There are a number of assumptions in our modeling approach that should be kept in mind for  
340 future comparisons against observations or more complex models. First, we did not account for  
341 silicate limitation. The latter is the main limiting factor for diatoms during late summer in Sub-  
342 Antarctic waters of the Southern Ocean (Leblanc et al, 2005). Changes in summer MLD might  
343 have a role on re-supplying silicate and alter diatoms summer production. Second, the  
344 biogeochemical model used here simulates iron remineralization in a simplistic way (Amount  
345 and Bopp, 2006). In our analysis we did not detect any significant change in summer iron  
346 concentration associated to remineralization. But it is possible that the representation of this  
347 mechanism in our model is too simplistic, because remineralization has been identified as a  
348 significant source of iron during summer in the Southern Ocean (Tagliabue et al, 2014 and  
349 2017). How changes in summer mixed-layer depth influence remineralization is out of scope of  
350 the current study but together with silicate limitation, these mechanisms could either compensate  
351 or intensify the summer trends presented here. Third, we made the choice to not consider  
352 changes in incoming solar radiation, and used clear-sky conditions at 45°S latitude in all our  
353 experiments. At higher latitudes, where incoming solar radiation is lower, we would expect to  
354 find shallower threshold depths, although this could be compensated by higher iron demand by  
355 phytoplankton. More difficult is to anticipate the impacts of a non-clear-sky over phytoplankton  
356 growth, as incoming solar radiation is simultaneously influenced by seasonal and intra-seasonal  
357 variability of cloud coverage, typology of clouds (type and altitude in the atmosphere) and sea-  
358 state (surface waves and bubbles). Fourth, we considered changes in MLD but we did not take  
359 into account the associated changes in temperature and wind stress. The former is particularly  
360 interesting, as laboratory experiments have recently shown interactive effects between iron and  
361 temperature for Southern Ocean diatoms (Hutchins and Boyd, 2016). Last, our study is based on  
362 a biogeochemical model that, despite its complexity, remains a simplification of the processes  
363 regulating phytoplankton growth. For instance, community structure was only represented in  
364 terms of size but it is well known that different phytoplankton species of similar sizes respond  
365 differently to environmental changes (Arrigo et al., 1999). Also, our model did not account for  
366 the potential contribution of vertically migrating zooplankton and small nekton to the carbon  
367 export. We should note however that, despite these assumptions, the relationships between  
368 primary production and MLD that came out of this modeling study are consistent with that

369 suggested from in-situ observations (Ardyna et al 2017, Hoppe et al 2017). Moreover, the  
370 analysis of a large ensemble of simulations also supports the robustness of our conclusions.

371 In conclusion, the results presented here provide a new and more refined explanation of the  
372 influence of MLD over Southern Ocean primary production and export. They provide a  
373 framework to analyze current and future patterns of production and export, in particular for  
374 CMIP6 projections and multiannual time-series obtained from *in-situ* observations such as  
375 moorings or BGC-Argo floats.

### 376 **Acknowledgments**

377 We thank Laurent Bopp, Christian Ethé, Julien LeSommer and Olivier Aumont for the technical  
378 support and insightful comments that strongly benefited this study. We also thank the two  
379 anonymous reviewers who took the time to review this work. We would like to acknowledge  
380 support from Sorbonne Université through the project PERSU. This study also benefited from  
381 the staff-exchange project SOCCLI, funded by EU (FP7-PEOPLE-2012-IRSES) and the  
382 SOBUMS project, funded by the Agence Nationale de la Recherche (ANR-16-CE01-0014). The  
383 ensemble of model outputs used in this study can be freely accessed at:  
384 <https://metadata.imas.utas.edu.au/geonetwork/srv/eng/main.home> ; and the PISCES code specific  
385 for the model configuration used in this study is available at <https://github.com/jllort>.

386



387 **References**

- 388 Ardyna, M., Claustre, H., Sallée, J.-B., D'Ovidio, F., Gentili, B., van Dijken, G., et al., 2017.  
389 Delineating environmental control of phytoplankton biomass and phenology in the Southern  
390 Ocean: Phytoplankton Dynamics in the SO. *Geophysical Research Letters* 44, 5016–5024.  
391 <https://doi.org/10.1002/2016GL072428>
- 392 Arrigo, K.R., Robinson, D.H., Worthen, D.L., Dunbar, R.B., DiTullio, G.R., VanWoert, M.,  
393 Lizotte, M.P., 1999. Phytoplankton Community Structure and the Drawdown of Nutrients and  
394 CO<sub>2</sub> in the Southern Ocean. *Science* 283 (5400): 365–67.  
395 <https://doi.org/10.1126/science.283.5400.365>.
- 396 Aumont, O., Bopp, L., 2006. Globalizing Results from Ocean in Situ Iron Fertilization Studies,  
397 *Global Biogeochemical Cycles* 20 (2), 20-2, <https://doi.org/10.1029/2005GB002591>.
- 398 Bissinger, J.E., Montagnes, D.J.S., Harples, J., Atkinson, D., 2008. Predicting marine  
399 phytoplankton maximum growth rates from temperature: Improving on the Eppley curve using  
400 quantile regression. *Limnol. Oceanogr.* 53, 487–493. <https://doi.org/10.4319/lo.2008.53.2.0487>
- 401 Bopp, L., Resplandy, L., Orr, J.C., Doney, S.C., Dunne, J.P., Gehlen, M., et al., 2013. Multiple  
402 stressors of ocean ecosystems in the 21st century: projections with CMIP5 models.  
403 *Biogeosciences* 10, 6225–6245. <https://doi.org/10.5194/bg-10-6225-2013>
- 404 Boyd, P.W., Strzepek, R., Fu, F., Hutchins, D.A., 2010. Environmental control of open-ocean  
405 phytoplankton groups: Now and in the future. *Limnology and Oceanography* 55, 1353–1376.  
406 <https://doi.org/10.4319/lo.2010.55.3.1353>
- 407 Boyd, P.W., Trull, T.W., 2007. Understanding the export of biogenic particles in oceanic waters:  
408 Is there consensus? *Progress in Oceanography* 72, 276–312.  
409 <https://doi.org/10.1016/j.pocean.2006.10.007>
- 410 Bracegirdle, T.J., Shuckburgh, E., Sallée, J.B., Wang, Z., Meijers, A. J. S., Bruneau, N., et al.,  
411 2013: Assessment of surface winds over the Atlantic, Indian and Pacific Ocean sectors of the  
412 Southern Hemisphere in CMIP5 models: historical bias, forcing response, and state dependence,

413 Journal of Geophysical Research - Atmospheres, 118, 547–562,  
414 <https://doi.org/10.1002/jgrd.50153>

415 Cai, W., Shi, G., Cowan, T., Bi, D., Ribbe, J., 2005. The response of the Southern Annular  
416 Mode, the East Australian Current, and the southern mid-latitude ocean circulation to global  
417 warming. *Geophysical Research Letters* 32. <https://doi.org/10.1029/2005GL024701>

418 Cisewski, B., Volker, H. S., and Hartmut, P. 2005. Upper-Ocean Vertical Mixing in the Antarctic  
419 Polar Front Zone. *Deep Sea Research Part II: Topical Studies in Oceanography*, Observations  
420 and modelling of mixed layer turbulence: Do they represent the same statistical quantities?, 52  
421 (9): 1087–1108. <https://doi.org/10.1016/j.dsr2.2005.01.010>.

422 Deppeler, S.L., Davidson, A.T., 2017. Southern Ocean Phytoplankton in a Changing Climate.  
423 *Front. Mar. Sci.* 4. <https://doi.org/10.3389/fmars.2017.00040>

424 Doney, S.C., 2006. Oceanography: Plankton in a warmer world. *Nature* 444, 695–696.  
425 <https://doi.org/10.1038/444695a>

426 D’Ortenzio, F., Antoine, D., Martinez, E., Ribera d’Alcalà, M., 2012. Phenological changes of  
427 oceanic phytoplankton in the 1980s and 2000s as revealed by remotely sensed ocean-color  
428 observations, *Global Biogeochemical Cycles* 26, n/a-n/a. <https://doi.org/10.1029/2011GB004269>

429 Eppley, R.W., 1972. Temperature and phytoplankton growth in the sea. *Fishery Bulletin* 70.

430 Hauck, J., C. Völker, D. A. Wolf-Gladrow, C. Laufkötter, M. Vogt, O. Aumont, L. Bopp, et al.  
431 2015. On the Southern Ocean CO<sub>2</sub> Uptake and the Role of the Biological Carbon Pump in the  
432 21st Century. *Global Biogeochemical Cycles* 29 (9): 1451–70.  
433 <https://doi.org/10.1002/2015GB005140>.

434 Henson, S. A., Sarmiento, J. L. , Dunne, J. P., Bopp, L. , Lima, I., Doney, S. C. , John, J. and  
435 Beaulieu, C. 2010. Detection of Anthropogenic Climate Change in Satellite Records of Ocean  
436 Chlorophyll and Productivity, *Biogeosciences* 7 (2): 621–40. <https://doi.org/10.5194/bg-7-621-2010>.

437 Henson, S.A., Yool, A., Sanders, R., 2015. Variability in efficiency of particulate organic carbon  
438 export: A model study, *Global Biogeochemical Cycles* 29, 33–45.  
439 <https://doi.org/10.1002/2014GB004965>

440 Hoppe, C.J.M., Klaas, C., Ossebaar, S., Soppa, M.A., Cheah, W., Laglera, L.M., et al., 2017.  
441 Controls of primary production in two phytoplankton blooms in the Antarctic Circumpolar  
442 Current., *Deep Sea Research Part II: Topical Studies in Oceanography*.  
443 <https://doi.org/10.1016/j.dsr2.2015.10.005>

444 Hutchins, D. A., and P. W. Boyd. 2016. Marine Phytoplankton and the Changing Ocean Iron  
445 Cycle. *Nature Climate Change* 6 (12): 1072–79. <https://doi.org/10.1038/nclimate3147>.

446 Jeandel, C, Ruiz-Pino, D., Gjata, E., Poisson, A., Brunet, C., Charriaud, E., et al., 1998.  
447 KERFIX, a Time-Series Station in the Southern Ocean: A Presentation. *Journal of Marine*  
448 *Systems* 17 (1–4): 555–69. [https://doi.org/10.1016/S0924-7963\(98\)00064-5](https://doi.org/10.1016/S0924-7963(98)00064-5).

449 Laufkötter, C., Vogt, M., Gruber, N., Aita-Noguchi, M., Aumont, O., Bopp, L., et al., 2015.  
450 Drivers and uncertainties of future global marine primary production in marine ecosystem  
451 models. *Biogeosciences* 12, 6955–6984. <https://doi.org/10.5194/bg-12-6955-2015>

452 Laufkötter, C., Vogt, M., Gruber, N., Aumont, O., Bopp, L., Doney, S.C., et al., 2016. Projected  
453 decreases in future marine export production: the role of the carbon flux through the upper ocean  
454 ecosystem. *Biogeosciences* 13, 4023–4047. <https://doi.org/10.5194/bg-13-4023-2016>

455 Lenton, A., Matear, R.J., 2007. Role of the Southern Annular Mode (SAM) in Southern Ocean  
456 CO<sub>2</sub> uptake. *Global Biogeochemical Cycles* 21, GB2016. <https://doi.org/10.1029/2006GB002714>

457 Leung, S., Cabré, A., Marinov, I., 2015. A latitudinally banded phytoplankton response to 21st  
458 century climate change in the Southern Ocean across the CMIP5 model suite. *Biogeosciences* 12,  
459 5715–5734. <https://doi.org/10.5194/bg-12-5715-2015>

460 Lévy, Marina. 2015. Exploration of the Critical Depth Hypothesis with a Simple NPZ Model.  
461 *ICES Journal of Marine Science* 72 (6): 1916–25. <https://doi.org/10.1093/icesjms/fsv016>.

462 Llorc, J., Lévy, M., Sallée, J.-B., Tagliabue, A., 2015. Onset, intensification, and decline of  
463 phytoplankton blooms in the Southern Ocean. *ICES Journal of Marine Science: Journal du*  
464 *Conseil* 72, 1971–1984. <https://doi.org/10.1093/icesjms/fsv053>

465 Lovenduski, N.S., Gruber, N., n.d. Impact of the Southern Annular Mode on Southern Ocean  
466 circulation and biology. *Geophysical Research Letters* 32. <https://doi.org/10.1029/2005GL022727>

467 Nicholson, S.-A., Lévy, M., Llorc, J., Swart, S., Monteiro, P.M.S., 2016. Investigation into the  
468 impact of storms on sustaining summer primary productivity in the Sub-Antarctic Ocean.  
469 *Geophys. Res. Lett.* 2016GL069973. <https://doi.org/10.1002/2016GL069973>

470 Panassa, E., C. Völker, D. Wolf-Gladrow, and J. Hauck. 2018. Drivers of Interannual Variability  
471 of Summer Mixed Layer Depth in the Southern Ocean Between 2002 and 2011 *Journal of*  
472 *Geophysical Research: Oceans* 123 (8): 5077–90. <https://doi.org/10.1029/2018JC013901>.

473 Pellichero, V., Sallée, J.-B., Schmidtko, S., Roquet, F., Charrassin, J.-B., 2017. The ocean mixed  
474 layer under Southern Ocean sea-ice: Seasonal cycle and forcing. *Journal of Geophysical*  
475 *Research: Oceans* 122, 1608–1633. <https://doi.org/10.1002/2016JC011970>

476 Sallée, J.B., Shuckburgh, E., Bruneau, N., Meijers, A.J.S., Bracegirdle, T.J., Wang, Z., 2013.  
477 Assessment of Southern Ocean mixed-layer depths in CMIP5 models: Historical bias and forcing  
478 response. *Journal of Geophysical Research: Oceans* 118, 1845–1862.  
479 <https://doi.org/10.1002/jgrc.20157>

480 Sallée, J.B., Speer, K.G., Rintoul, S.R., 2010. Zonally asymmetric response of the Southern  
481 Ocean mixed-layer depth to the Southern Annular Mode. *Nature Geoscience* 3, 273–279.  
482 <https://doi.org/10.1038/ngeo812>

483 Sarmiento, J. L., R. Slater, R. Barber, L. Bopp, S. C. Doney, A. C. Hirst, J. Kleypas, et al. 2004.  
484 Response of Ocean Ecosystems to Climate Warming. *Global Biogeochemical Cycles* 18 (3):  
485 GB3003. <https://doi.org/10.1029/2003GB002134>.

486 Schourup-Kristensen, V., 2015. Iron in the Southern Ocean: Spatial distribution and the effect on  
487 the phytoplankton. Bremen University, Alfred-Wegener-Institute. <http://epic.awi.de/38667/>

488 Siegel, D.A., Behrenfeld, M.J., Maritorena, S., McClain, C.R., Antoine, D., Bailey, S.W., et al.,  
489 2013. Regional to global assessments of phytoplankton dynamics from the SeaWiFS mission.  
490 *Remote Sensing of Environment* 135, 77–91. <https://doi.org/10.1016/j.rse.2013.03.025>

491 Swart, N.C., Fyfe, J.C., Gillett, N., Marshall, G.J., 2015. Comparing Trends in the Southern  
492 Annular Mode and Surface Westerly Jet. *J. Climate* 28, 8840–8859. [https://doi.org/10.1175/JCLI-D-](https://doi.org/10.1175/JCLI-D-15-0334.1)  
493 [15-0334.1](https://doi.org/10.1175/JCLI-D-15-0334.1)

494 Swart, N.C., Gille, S.T., Fyfe, J.C. and Gillett, N.P. 2018. Recent Southern Ocean Warming and  
495 Freshening Driven by Greenhouse Gas Emissions and Ozone Depletion. *Nature Geoscience* 11  
496 (11): 836. <https://doi.org/10.1038/s41561-018-0226-1>.

497 Tagliabue, A., Bowie, A.R., Boyd, P.W., Buck, K.N., Johnson, K.S., Saito, M.A., 2017. The  
498 integral role of iron in ocean biogeochemistry. *Nature* 543, 51–59. <https://doi.org/10.1038/nature21058>

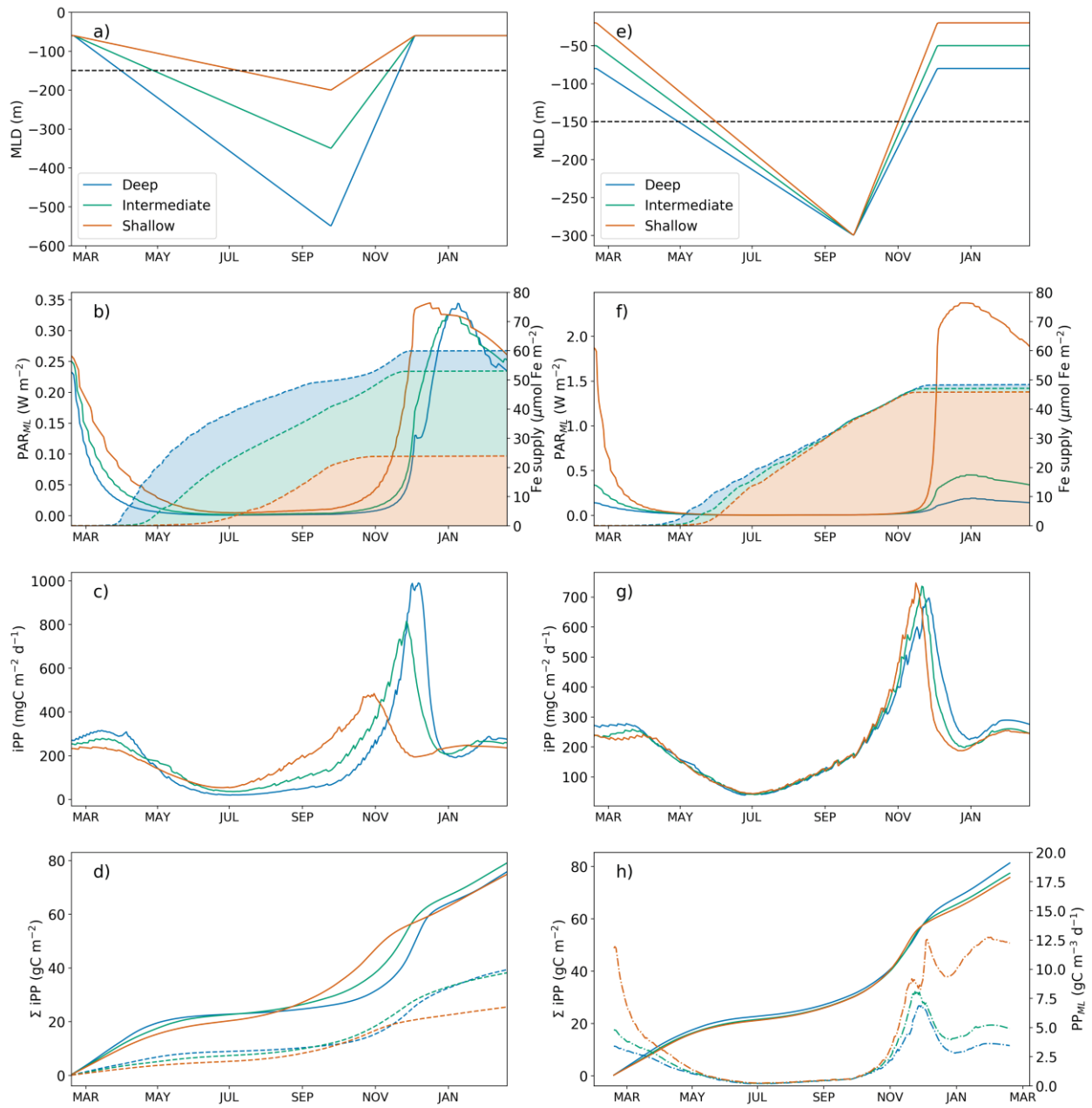
499 Tagliabue, A., T. Mtshali, O. Aumont, A. R. Bowie, M. B. Klunder, A. N. Roychoudhury, and S.  
500 Swart. 2012. A Global Compilation of Dissolved Iron Measurements: Focus on Distributions and  
501 Processes in the Southern Ocean, *Biogeosciences* 9 (6): 2333–49. [https://doi.org/10.5194/bg-9-2333-](https://doi.org/10.5194/bg-9-2333-2012)  
502 [2012](https://doi.org/10.5194/bg-9-2333-2012).

503 Tagliabue, A., Sallée, J.-B., Bowie, A.R., Lévy, M., Swart, S., Boyd, P.W., 2014. Surface-water  
504 iron supplies in the Southern Ocean sustained by deep winter mixing. *Nature Geoscience* 7, 314–  
505 320. <https://doi.org/10.1038/ngeo2101>

506 Takao, S., Hirawake, T., Wright, S.W., Suzuki, K., 2012. Variations of net primary productivity  
507 and phytoplankton community composition in the Southern Ocean as estimated from ocean-color  
508 remote sensing data. *Biogeosciences Discussions* 9, 4361–4398. [https://doi.org/10.5194/bgd-9-4361-](https://doi.org/10.5194/bgd-9-4361-2012)  
509 [2012](https://doi.org/10.5194/bgd-9-4361-2012)

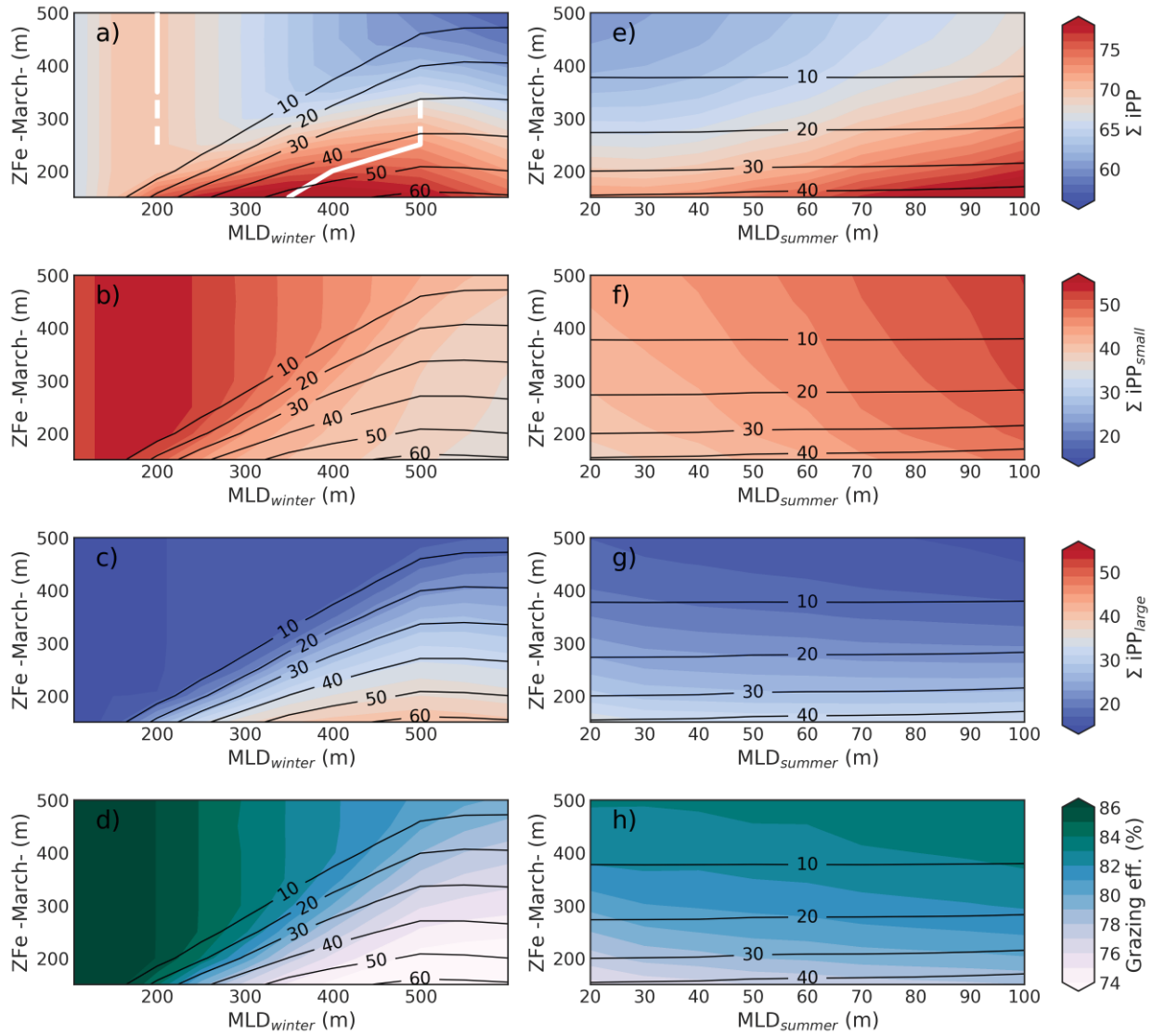
510 Taylor, K.E., Stouffer, R.J., Meehl, G.A., 2012. An Overview of CMIP5 and the Experiment  
511 Design. *Bulletin of the American Meteorological Society* 93, 485–498.  
512 <https://doi.org/10.1175/BAMS-D-11-00094.1>

513 Zheng, F., Li, J., Clark, R.T., Nnamchi, H.C., 2013. Simulation and Projection of the Southern  
514 Hemisphere Annular Mode in CMIP5 Models. *Journal of Climate* 26, 9860–9879.  
515 <https://doi.org/10.1175/JCLI-D-13-00204.1>  
516



518

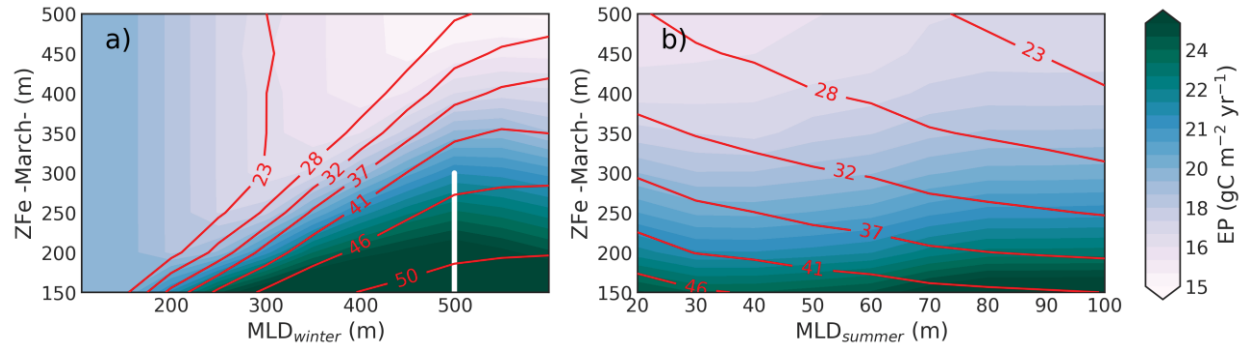
519



520

521





522

523

524 CAPTIONS

525 **Figure 1:** Left panels: Seasonal cycles of (a) mixed layer depth, (b) averaged PAR in the MLD (plain lines) and  
526 time-cumulative vertical supply of iron (dashed contours with colors filled) into the MLD, (c) depth-integrated  
527 primary production (iPP), and (d) time-cumulative integrated primary production ( $\Sigma$ iPP, plain lines) and integrated  
528 primary production for the large-phytoplankton group (dashed lines) for three simulations with identical  $Z_{Fe}$  depth  
529 and  $MLD_{summer}$  but with different  $MLD_{winter}$ . The black dashed line in (a) indicates the value of  $Z_{Fe}$ . Right panels:  
530 same but for simulations runs with identical  $Z_{Fe}$  depth and  $MLD_{winter}$  and different  $MLD_{summer}$ . In h), dash-dotted  
531 lines represent primary production averaged in the mixed-layer ( $PP_{ML}$ ).

532 **Figure 2:** Left panels: a) Annual integrated Primary Production (in  $gC\ m^{-2}\ yr^{-1}$ ) as a function of initial Ferricline  
533 depth ( $Z_{Fe}$ ) and winter MLD ( $MLD_{winter}$ ). White solid lines indicate threshold depths ( $Z_{PPmax}$ ) and white dashed lines  
534 indicate the range where two different thresholds were detected. c) Same as a) but for small phytoplankton. c) Same  
535 as a) but for large phytoplankton. d) Portion of annual primary production grazed by zooplankton (grazing  
536 efficiency). In all panels, the black contours show the vertical supply of iron (nmolFe/yr). Right panels: same, but  
537 against summer MLD ( $MLD_{summer}$ ).

538 **Figure 3:** a) Annual Primary Production exported below 100m depth as a function of initial Ferricline depth ( $Z_{Fe}$ )  
539 and winter MLD ( $MLD_{winter}$ ). Red contours show the percentage of primary production done by the large (and fast-  
540 sinking) phytoplankton. The white line indicates the threshold depth for EP-MLD relationship. b) Same as a) but  
541 against summer MLD ( $MLD_{summer}$ ).

542

Figure 1.

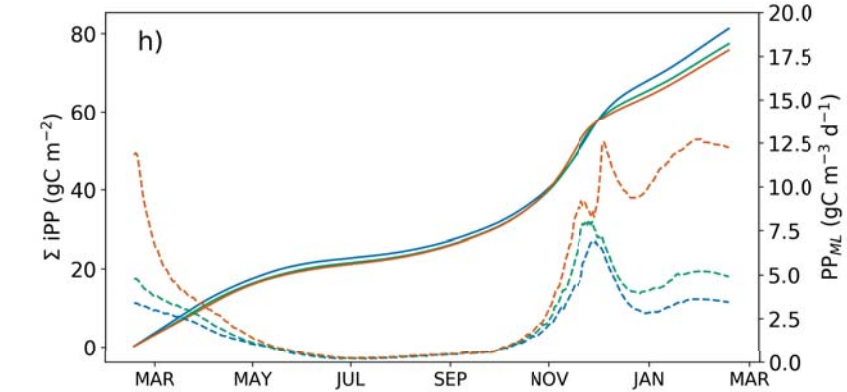
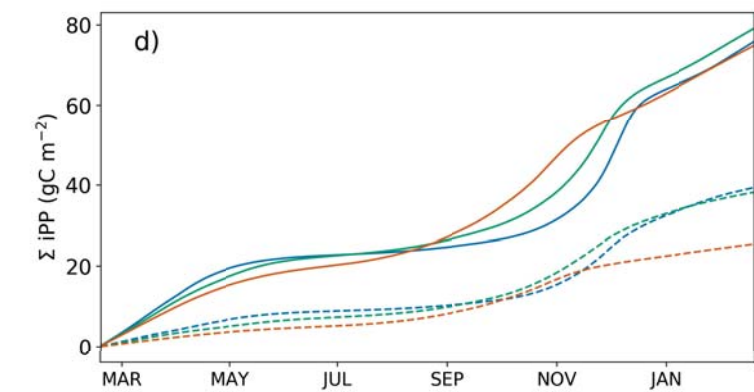
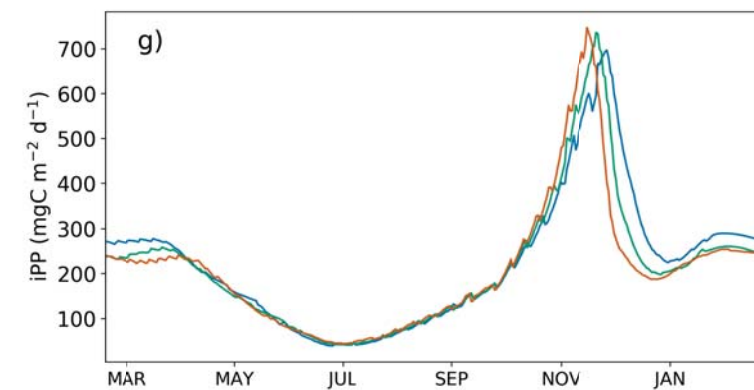
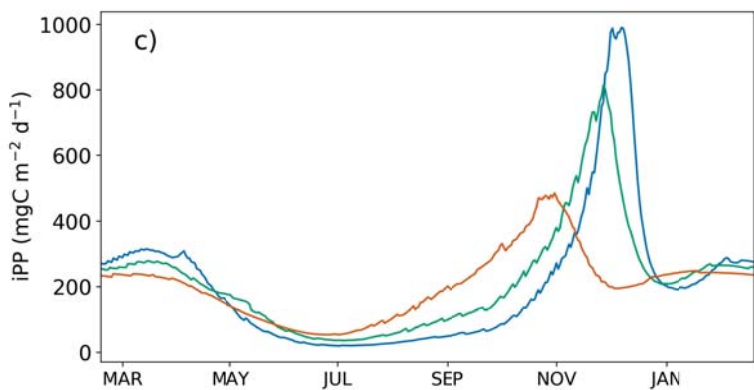
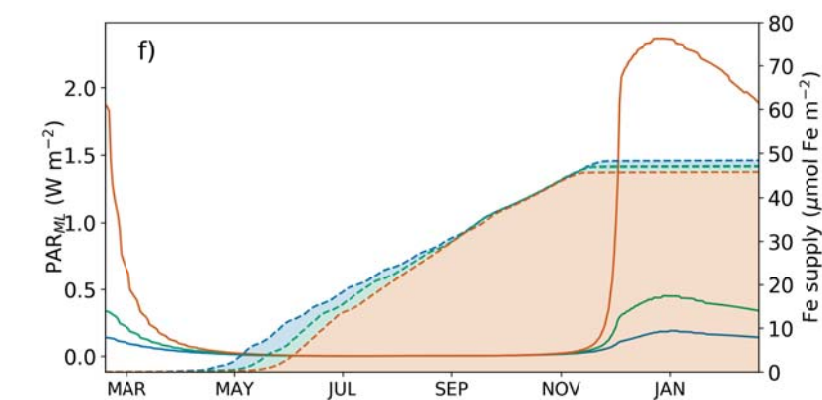
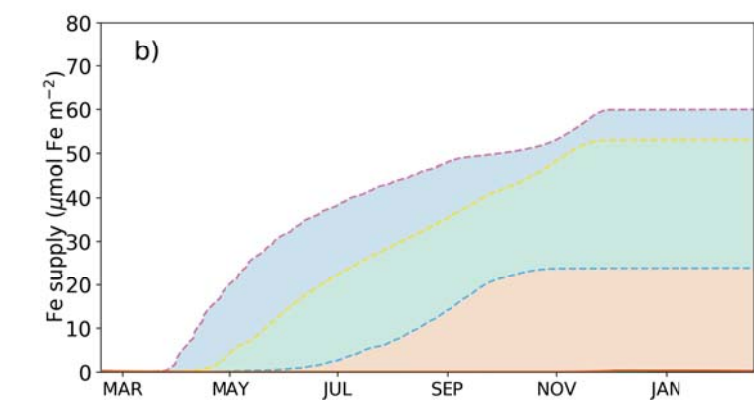
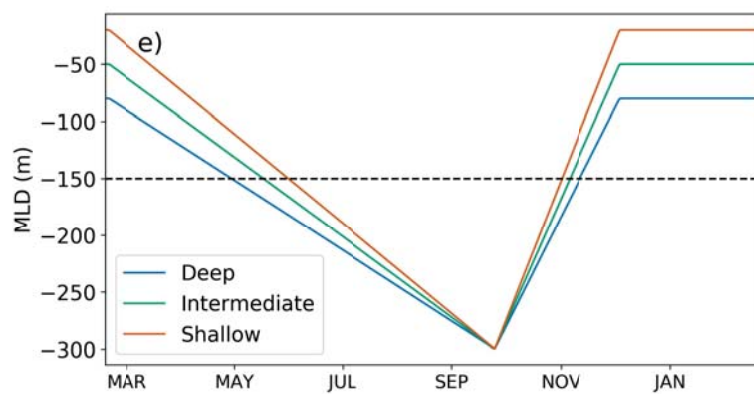
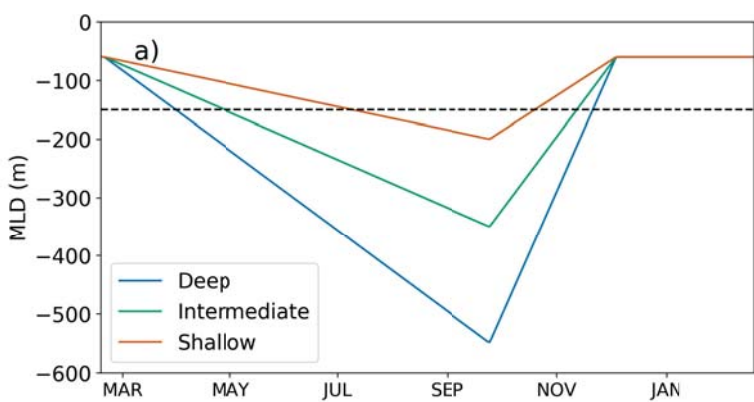


Figure 2.

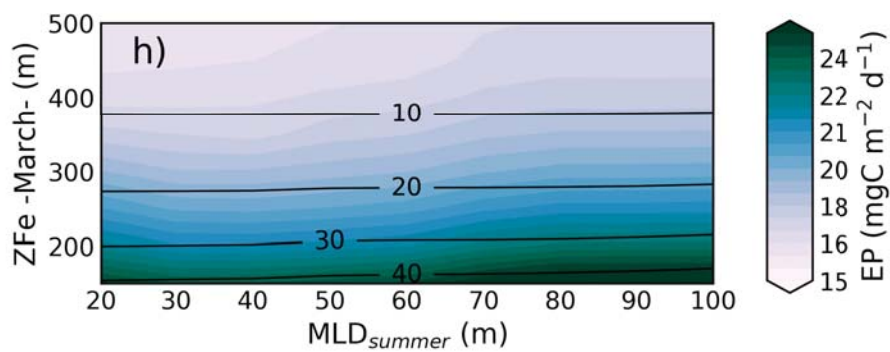
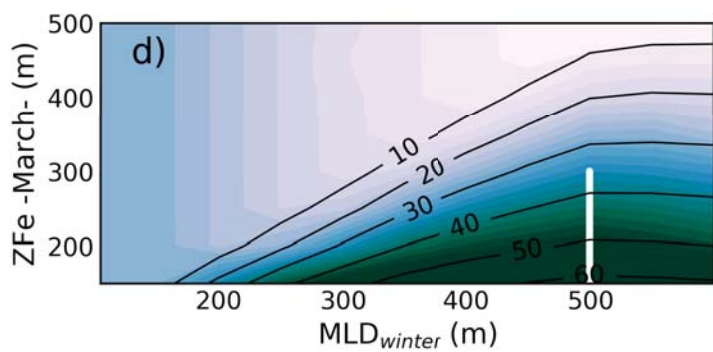
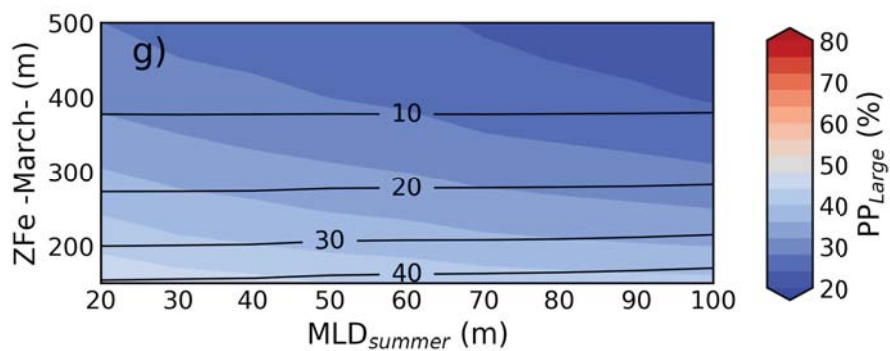
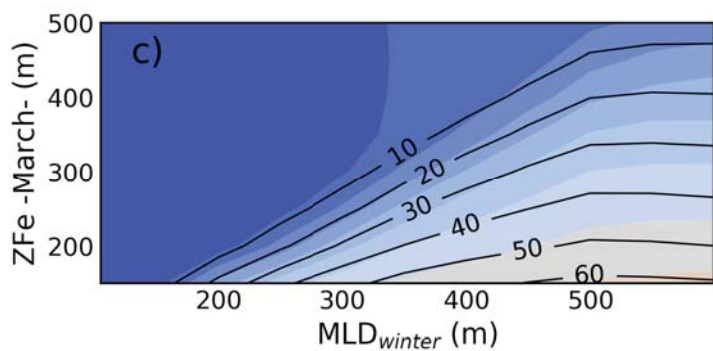
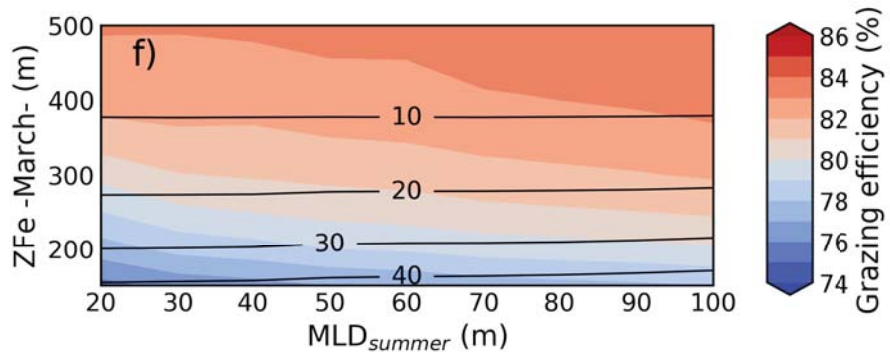
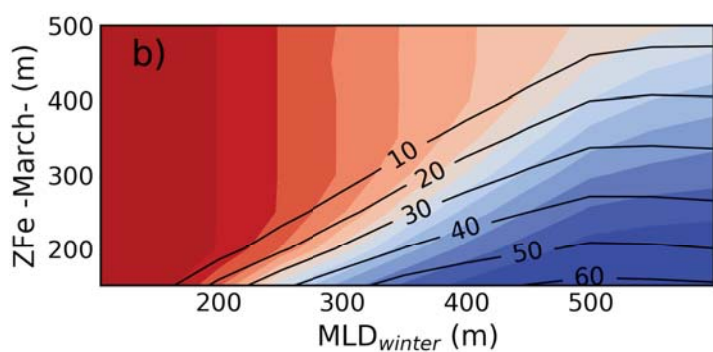
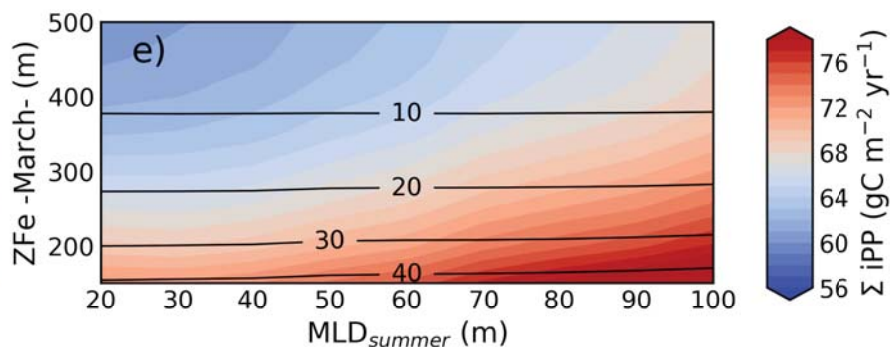
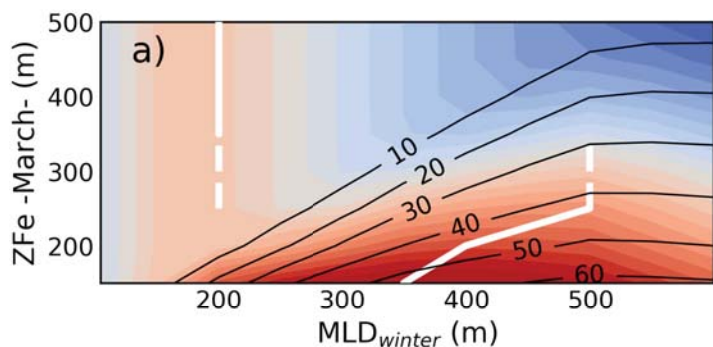


Figure 3.

